

# High-harmonic generation by resonant plasmon field enhancement

Seungchul Kim<sup>1\*</sup>, Jonghan Jin<sup>1\*</sup>, Young-Jin Kim<sup>1</sup>, In-Yong Park<sup>1</sup>, Yunseok Kim<sup>1</sup> & Seung-Woo Kim<sup>1</sup>

High-harmonic generation by focusing a femtosecond laser onto a gas is a well-known method of producing coherent extreme-ultraviolet (EUV) light<sup>1–3</sup>. This nonlinear conversion process requires high pulse intensities, greater than  $10^{13} \text{ W cm}^{-2}$ , which are not directly attainable using only the output power of a femtosecond oscillator. Chirped-pulse amplification enables the pulse intensity to exceed this threshold by incorporating several regenerative and/or multi-pass amplifier cavities in tandem<sup>4,5</sup>. Intracavity pulse amplification (designed not to reduce the pulse repetition rate) also requires a long cavity<sup>6,7</sup>. Here we demonstrate a method of high-harmonic generation that requires no extra cavities. This is achieved by exploiting the local field enhancement induced by resonant plasmons within a metallic nanostructure consisting of bow-tie-shaped gold elements on a sapphire substrate. In our experiment, the output beam emitted from a modest femtosecond oscillator (100-kW peak power, 1.3-nJ pulse energy and 10-fs pulse duration) is directly focused onto the nanostructure with a pulse intensity of only  $10^{11} \text{ W cm}^{-2}$ . The enhancement factor exceeds 20 dB, which is sufficient to produce EUV wavelengths down to 47 nm by injection with an argon gas jet. The method could form the basis for constructing laptop-sized EUV light sources for advanced lithography and high-resolution imaging applications.

Field enhancement is attributed to the collective motion of free electrons confined in narrowly localized regions, similar to that

observed in colloidal nanoparticles exposed to an external electromagnetic field<sup>8,9</sup>. For the given geometry of a nanoparticle or nanostructure, the degree of field enhancement induced by resonant plasmons can be estimated by solving Maxwell's equations analytically<sup>10</sup> or numerically<sup>11</sup>. Using appropriate fabrication techniques, it is consequently possible to optimize the shape of a nanostructure to be tailored to a particular application<sup>12–15</sup>. We adopted this approach in the present investigation, to design and build a nanostructure that enables the generation of high harmonics from a modest femtosecond oscillator through field enhancement around the nanostructure.

Figure 1 illustrates the construction of the experimental apparatus. The femtosecond oscillator used here is a titanium-sapphire oscillator (Femtosource sPRO, Femtolasers) set to emit a train of 10-fs pulses of 800-nm carrier wavelength at a repetition rate of 75 MHz. The output beam from the oscillator has a small peak power of  $\sim 100 \text{ kW}$  and each pulse has an energy of 1.3 nJ, yielding a pulse intensity of only  $\sim 10^{11} \text{ W cm}^{-2}$  even when well focused. The pulse intensity must be increased at least by two orders of magnitude to reach the threshold required to generate high harmonics by interaction with a gas jet. To do this, a metallic nanostructure consisting of a two-dimensional array of gold 'bow tie' elements on a sapphire plate is inserted in the focal plane of the focused beam.

The pulse intensity builds up when the femtosecond pulse passes through the nanostructure. The degree of field enhancement is

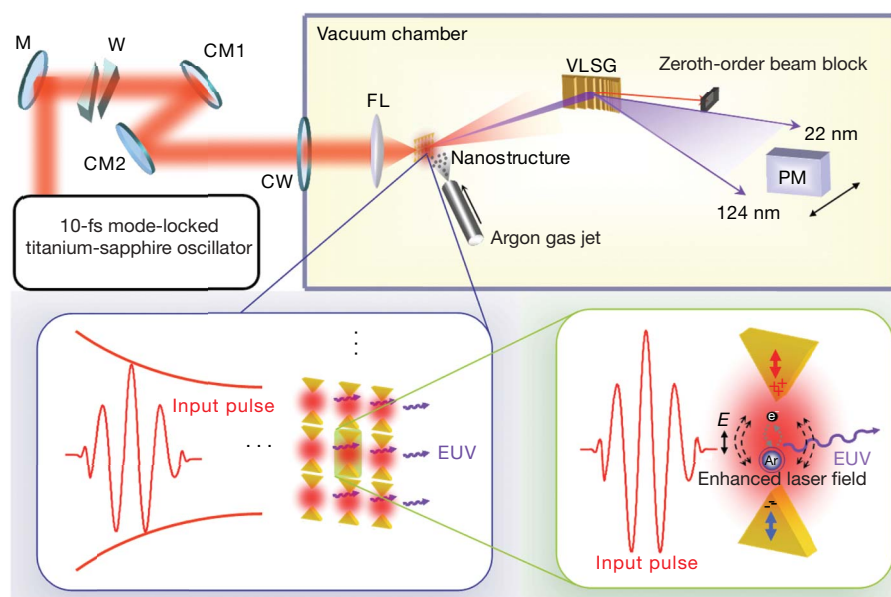


**Figure 1 | Apparatus for high-harmonic generation by electric field enhancement using a nanostructure of bow-tie elements.**

Anticlockwise from top: the overall system configured for the experiment, a detailed view of the two-dimensional array of bow-tie elements fabricated on a sapphire plate, and the magnified view of a single gold bow-tie element interacting with the incident pulse. Ar, argon atom; CM, chirped mirror; CW, chamber window; FL, focusing lens; M, mirror; PM, photon multiplier; VLSG, varied-line-spacing grating; W, wedge plate; E, electric field.

<sup>1</sup>Billionth Uncertainty Precision Engineering Group, KAIST, Daedeok Science Town, Daejeon 305-701, South Korea.

\*These authors contributed equally to this work.

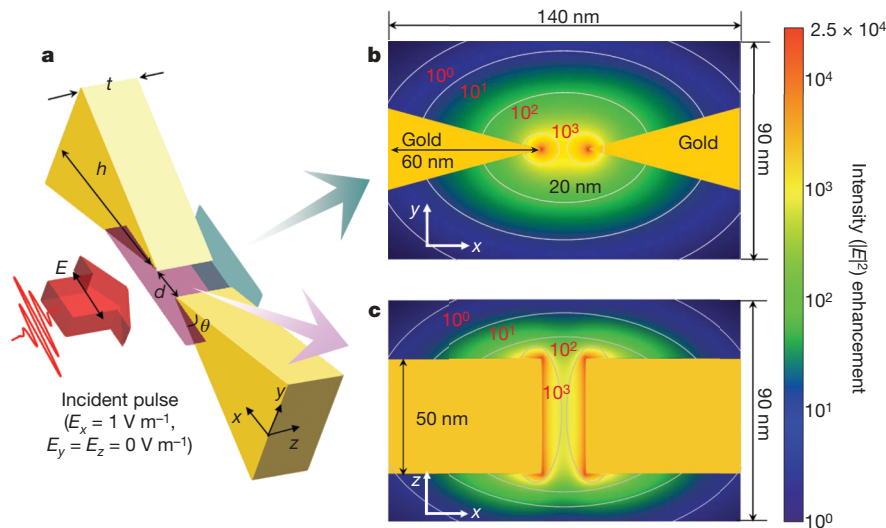


**Figure 2 | Finite-difference time-domain simulation of local field enhancement.** **a**, Geometrical conditions for simulation of a single bow-tie element. The polarization direction of the incident pulse parallel to the  $x$ - $z$  plane. **b**, Intensity field computed in the  $x$ - $y$  plane. **c**, Same simulation result

significantly affected by the geometrical shape of the nanostructure, as revealed in previous investigations of different shapes of particles, wires, and tips<sup>16–19</sup>. The bow-tie shape of the nanostructure elements—a pair of triangular patches placed apex to apex with a small gap between them—is taken as the nanostructure's basic feature. When exposed to the femtosecond pulse, free electrons are confined within one apex of the bow-tie element and the opposing apex is filled with positive charges, which makes the pulse capable of producing a strong field enhancement between the vertices.

As illustrated in Fig. 2, the bow-tie shape is characterized by four geometrical parameters, the thickness ( $t$ ), angle ( $\theta$ ), gap ( $d$ ) and height ( $h$ ). These parameters must be selected so as to maximize the resulting field enhancement. For this, the finite-difference time-domain method was adopted<sup>20,21</sup>, and Maxwell's equations for the case shown in Fig. 2a were numerically solved. The polarization direction of the incident femtosecond pulse is positioned parallel to the line connecting the vertices. The incident pulse is assumed to have a bandwidth of 100 nm about the 800-nm carrier wavelength. The wavelength-dependent dielectric constant of the tip material, gold, was determined using the modified Debye model<sup>22</sup>. Through trial-and-error simulation, the four parameters were finally determined as follows:  $h = 175$  nm,  $d = 20$  nm,  $t = 50$  nm and  $\theta = 30^\circ$ . The corresponding field enhancement was computed as shown in Figs 2b and 2c. The entire volume of simulation, including a bow-tie element, was evenly divided into hexahedral grids  $1$  nm  $\times$   $1$  nm  $\times$   $1$  nm in size. No singularity effect along the edge line of the element was considered. The computation shows that the intensity enhancement factor reaches its maximum, 44 dB, at the vertices. In addition, within the  $60$  nm  $\times$   $50$  nm  $\times$   $50$  nm ( $x \times y \times z$ ) region in the gap between the vertices, the enhancement factor is greater than 20 dB. This result confirms that the field enhancement suffices to boost the pulse intensity to well above the required threshold of  $10^{13}$  W cm<sup>-2</sup>, given that the input pulse has an intensity of  $10^{11}$  W cm<sup>-2</sup>.

The time-dependent dynamic behaviour of plasmon resonance within the nanostructure causes a temporal phase delay in the enhanced field in response to the original pulse. The simulation (Fig. 2) revealed a uniform phase delay of  $90^\circ$ , confirming the phase consistency over the entire enhanced field. In addition to gold, three other metals, silver, copper and platinum, were also considered. However, simulation showed that no significant difference existed in the resulting field enhancement, other than in platinum being less effective. Thus, we chose gold as the bow-tie

viewed in the  $x$ - $z$  plane. The design parameters selected were  $h = 175$  nm,  $d = 20$  nm,  $t = 50$  nm and  $\theta = 30^\circ$ . The intensity enhancement factor, which reached a maximum of  $2.5 \times 10^4$  at the apex of each triangle, turned out to be  $>10^2$  within the  $60$  nm  $\times$   $50$  nm  $\times$   $50$  nm ( $x \times y \times z$ ) volume in the gap.

material in consideration of our experience with the metal in nanofabrication.

Figure 3 shows a scanning electron microscope image of the nanostructure actually fabricated on a sapphire plate of 400- $\mu$ m thickness. Using the electron beam evaporation process, a 50-nm gold layer was deposited on a 5-nm chromium adhesion layer on the sapphire plate. By means of precise control of the focused ion beam, we then made bow-tie elements by scribing the deposited gold and chromium layers with subnanometer lateral resolution. The sapphire plate serves as a solid transparent substrate holding bow-tie elements in a two-dimensional array with a spatial pitch of 200 nm in one direction and 550 nm in the perpendicular direction, over a  $10$   $\mu$ m  $\times$   $10$   $\mu$ m area. The sapphire plate acts as a heat dissipator that protects the nanostructure from thermal damage both during nanofabrication

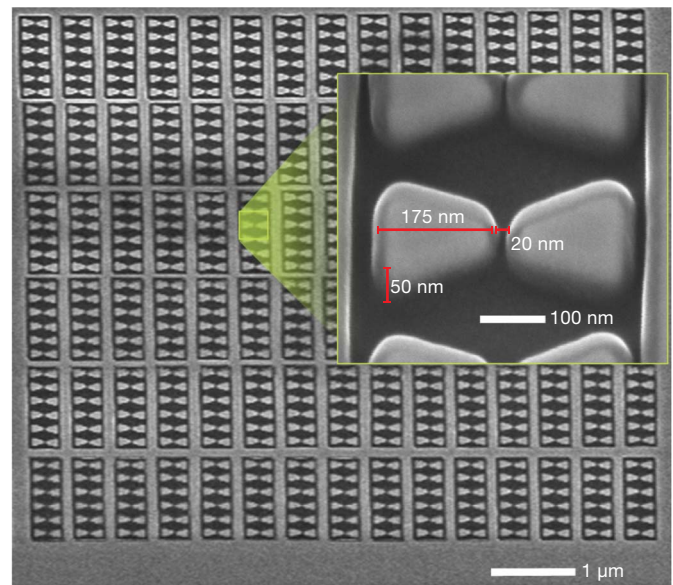


**Figure 3 | Scanning electron microscope image of the nanostructure used for high-harmonic generation.** Bow-tie elements were arranged in a two-dimensional,  $36 \times 15$  array with an area of  $10$   $\mu$ m  $\times$   $10$   $\mu$ m. The inset shows the magnified image of a single bow-tie element with the important dimensions marked. Owing to the high magnification, edge lines are seen blurred by multiple scattering of electrons in imaging.

and when it is illuminated by the femtosecond laser for high-harmonic generation.

As shown in Fig. 1, the sapphire plate was placed inside the vacuum chamber and the nanostructure was positioned to face the nozzle of the gas jet. The output beam of the femtosecond laser was fed into the vacuum chamber through a window and then focused on the nanostructure using an aspheric focusing lens. The group delay dispersion, which was caused by the chamber window, the focusing lens and the sapphire plate, and amounted to  $400 \text{ fs}^2$ , was compensated for using chirped mirrors together with a pair of wedges. Inside the chamber, a vacuum of  $10^{-4}$ – $10^{-5}$  torr was maintained by operating a rotary pump together with a diffusion pump equipped with a liquid nitrogen trap. The apparatus was placed on a granite table floated on air supports to prevent external vibration. A gas jet of argon was injected through a nozzle of 100- $\mu\text{m}$  diameter to provide a surface density of 0.29 g per litre by a back pressure of 115 torr.

To detect the generated high harmonics, a high-resolution spectrometer was constructed by combining a type of diffraction grating with varied line spacing (Hitachi, 001-0639) with a photon multiplier (Photonics, 4751G CSI). The photon multiplier was located at a distance of 469 mm from the grating, which dispersed the incoming EUV radiation in the 22–124-nm wavelength range along a transverse line 110 mm long. The photon multiplier was mounted on a precision stage moving along the dispersion line of the grating. The photon multiplier we used was sensitive to high-harmonic radiation only below 200 nm in wavelength; hence, no aluminium filters were required to block the original femtosecond laser beam. The grating has a narrow acceptance angle of  $\pm 1.0^\circ$ , which provides a 1.0-nm wavelength sampling resolution. In addition, a slit of 1.0-mm width was installed to limit the aperture size of the photon multiplier to avoid the effect of excessive convolution in the measured data.

Figure 4 shows the detection result obtained in this investigation. Odd harmonics up to the 17th, denoted H17, can be clearly seen. H3 and H5 are not seen, because they are below the lower limit of the dispersion range of the grating we used. The three-stage power variation usually seen in the harmonics generated by chirped power amplification was also observed<sup>23,24</sup>, as evidenced by a perturbative region from H7 to H11, a plateau from H11 to H15, and a final cutoff

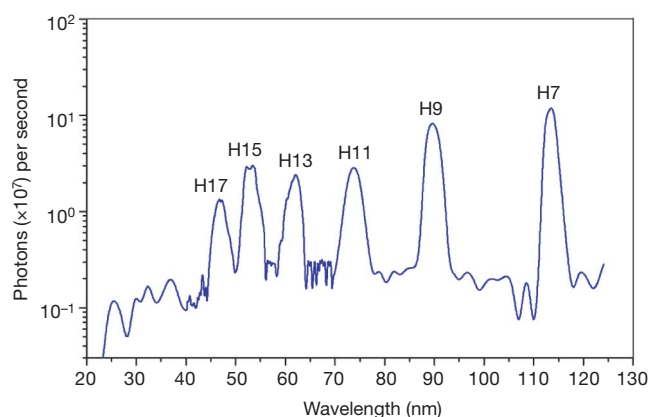


**Figure 4 | Measured spectrum of generated high harmonics.** A varied-line-spacing grating was used to disperse the 22–124-nm wavelength band over a total linear length of 110 mm. H7, H9 and H11 were monitored by moving a photon multiplier in steps of 1.0 mm along the dispersion line, and H13, H15 and H17 were monitored in steps of 0.2 mm. The aperture of the photon multiplier was adjusted to be 1.0 mm to reduce the unwanted convolution effect in the measured spectrum while maintaining a desirable level of photon-counting sensitivity. Given the input pulse power of 100 mW, the efficiencies for the harmonics were computed as follows: H7,  $2.4 \times 10^{-9}$ ; H9,  $2.2 \times 10^{-9}$ ; H11,  $9.5 \times 10^{-10}$ ; H13,  $9.0 \times 10^{-10}$ ; H15,  $1.3 \times 10^{-9}$ ; and H17,  $6.9 \times 10^{-10}$ .

at H17. Given that the input femtosecond laser provides a small peak power of 100 kW, the observed harmonics yield relatively low power, in the range of a few nanowatts in total. However, the conversion efficiency was found to be on the level of  $2.4 \times 10^{-9}$  for H7 and as low as  $6.9 \times 10^{-10}$  for H17, which is comparable to those of chirped power amplification. We expect that the original comb structure is maintained in each of the generated harmonics as there was no reduction in the repetition rate of the incident femtosecond pulses, although experimental verification of this is not within the scope of the current investigation.

Sapphire could break down owing to multiphoton ionization if it were exposed to an intensity of greater than  $10^{13} \text{ W cm}^{-2}$  (ref. 25). However, the sapphire substrate used in the experiment was found not to be substantially influenced, because the electric field exceeding the threshold intensity was concentrated within the gap between the triangular electrodes. This was verified by scanning electron microscope imaging after the experiment. The gold electrodes themselves are also susceptible to thermal damage owing to photon–electron coupling when the incident femtosecond pulse yields an intensity of greater than  $10^{11} \text{ W cm}^{-2}$  (ref. 26). Because the sapphire substrate functions as a good heat dissipator, no serious ablation or melting of the electrodes was observed, however, as long as the incident intensity was not allowed to exceed the threshold intensity.

Another concern was the spatial distribution shared by the high harmonics generated using the array of bow-tie elements. The intense spot of the incident femtosecond pulse focused on the surface of the nanostructure had a diameter of 5  $\mu\text{m}$ , which is large enough to produce high-harmonic generation simultaneously in approximately 150 of the elements. Each element acts as a point-like source that radiates high harmonics with a broad angle distribution. The consequent wave collectively observed from the elements is therefore the constructive interference of the individual waves emitted from the individual elements, which maintain high coherence in both spatial and temporal terms. This causes the generated harmonics to be distributed following the particular spatial diffraction pattern that the nanostructure would produce as a two-dimensional diffractive grating as a whole.

For instance, H17, which has a wavelength of 47 nm, has a first-order diffraction angle of  $13.6^\circ$  in one direction and  $4.9^\circ$  in the perpendicular direction, with greater higher-order diffraction. In the experiment, only the zeroth-order diffracted ray of H17 was collected by the photon multiplier, because the other diffraction angles are greater than the acceptance angle of  $\pm 1.0^\circ$  of the spectrometer used. This is the case for the other detected harmonics, H7–H15, as well. The zeroth-order diffracted rays of the generated harmonics all have the same propagation direction as the incident femtosecond pulse, and are thus confined within a narrow cone with a  $\pm 7^\circ$  angle distribution formed in response to the focusing angle of the incident pulse.

A final concern was the dispersion-induced phase mismatching due to the interaction of the generated harmonics with the injected argon gas. However, we did not pay particular attention to this problem, because the field enhancement for the high-harmonic generation was confined to region of dimension less than 1  $\mu\text{m}$  as the incident femtosecond pulse passed through the bow-tie elements.

In conclusion, in the experiment performed in this study we successfully verified that the field enhancement induced around the bow-tie elements with a 20-nm gap allows the generation of EUV light directly from the output of a single femtosecond oscillator of 100-kW peak power. The focused pulse intensity of  $10^{11} \text{ W cm}^{-2}$  was enhanced by a factor of 20–40 dB, which is large enough to produce harmonics as high as the 17th, corresponding to a wavelength of 47 nm. Requiring no extra cavities, the proposed method enables the construction of convenient laptop-size sources of coherent EUV radiation. This has the potential to accelerate progress in many areas of science and technology, particularly in the area of advanced

lithography, high-resolution imaging and possibly EUV optical clocks.

Received 28 January; accepted 11 April 2008.

1. Corkum, P. B. Plasma perspective on strong-field multiphoton ionization. *Phys. Rev. Lett.* **71**, 1994–1997 (1993).
2. Lewenstein, M., Balcou, P., Ivanov, M., Yu., L'Huillier, A. & Corkum, P. B. Theory of high-harmonic generation by low-frequency laser fields. *Phys. Rev. A* **49**, 2117–2132 (1994).
3. Chang, Z., Rundquist, A., Wang, H., Murnane, M. M. & Kapteyn, H. C. Generation of coherent soft X rays at 2.7 nm using high harmonics. *Phys. Rev. Lett.* **79**, 2967–2970 (1997).
4. Strickland, D. & Mourou, G. Compression of amplified chirped optical pulses. *Opt. Commun.* **56**, 219–221 (1985).
5. Seres, J. *et al.* Laser technology: Source of coherent kiloelectronvolt X-rays. *Nature* **433**, 596 (2005).
6. Gohle, C. *et al.* A frequency comb in the extreme ultraviolet. *Nature* **436**, 234–237 (2005).
7. Jones, R. J., Moll, K. D., Thorpe, M. J. & Ye, J. Phase-coherent frequency combs in the vacuum ultraviolet via high-harmonic generation inside a femtosecond enhancement cavity. *Phys. Rev. Lett.* **94**, 193201 (2005).
8. Nisoli, M. Nanoplasmonics: Brave new attoworld. *Nature Photon.* **1**, 499–500 (2007).
9. Roth, M. R., Panoiu, C. N., Adams, M. M. & Osgood, M. R. Jr. Resonant-plasmon field enhancement from asymmetrically illuminated conical metallic-probe tips. *Opt. Express* **14**, 2921–2931 (2006).
10. Schatz, G. C. & Van Duyne, R. P. *Handbook of Vibrational Spectroscopy* Vol. 1 (eds Chalmers, J. M. & Griffiths, P. R.) 759–774 (Wiley, Chichester, 2002).
11. Bohn, L. J., Nesbitt, J. D. & Gallagher, A. Field enhancement in apertureless near-field scanning optical microscopy. *J. Opt. Soc. Am. A* **18**, 2998–3006 (2001).
12. Mühlischlegel, P., Eisler, H.-J., Martin, O. J. F., Hecht, B. & Pohl, D. W. Resonant optical antennas. *Science* **308**, 1607–1609 (2005).
13. Bragas, A. V. & Martínez, O. E. Field-enhanced scanning optical microscope. *Opt. Lett.* **25**, 631–633 (2000).
14. Stockman, M. I. Nanofocusing of optical energy in tapered plasmonic waveguides. *Phys. Rev. Lett.* **93**, 137404 (2004).
15. Lesuffleur, A., Kumar, L. K. S. & Gordon, R. Enhanced second harmonic generation from nanoscale double-hole arrays in a gold film. *Appl. Phys. Lett.* **88**, 261104 (2006).
16. Jin, E. X. & Xu, X. Enhanced optical near field from a bowtie aperture. *Appl. Phys. Lett.* **88**, 153110 (2006).
17. Onuta, T.-D., Waagele, M., DuFort, C. C., Schaich, W. L. & Dragnea, B. Optical field enhancement at cusps between adjacent nanoapertures. *Nano Lett.* **7**, 557–564 (2007).
18. Sun, W.-X. & Shen, Z.-X. Optimizing the near field around silver tips. *J. Opt. Soc. Am. A* **20**, 2254–2259 (2003).
19. Tzeng, Y.-F. *et al.* Fabrication of an ultra-nanocrystalline diamond-coated silicon wire array with enhanced field-emission performance. *Nanotechnology* **18**, 435703 (2007).
20. Fromm, D. P., Sundaramurthy, A., James Schuck, P., Kino, G. & Moerner, W. E. Gap-dependent optical coupling of single “bowtie” nanoantennas resonant in the visible. *Nano Lett.* **4**, 957–961 (2004).
21. Krug, J. T. II, Sánchez, E. J. & Xie, X. S. Design of near-field optical probes with optimal field enhancement by finite difference time domain electromagnetic simulation. *J. Chem. Phys.* **116**, 10895–10901 (2002).
22. Gai, H., Wang, J. & Tian, Q. Modified Debye model parameters of metals applicable for broadband calculations. *Appl. Opt.* **46**, 2229–2233 (2007).
23. Zhou, J., Peatross, J., Murnane, M. M., Kapteyn, H. C. & Christov, I. P. Enhanced high-harmonic generation using 25 fs laser pulses. *Phys. Rev. Lett.* **76**, 752–755 (1996).
24. Wahlström, C.-G. *et al.* High-order harmonic generation in rare gases with an intense short pulse laser. *Phys. Rev. A* **48**, 4709–4720 (1993).
25. Wang, X. C. *et al.* Femtosecond pulse laser ablation of sapphire in ambient air. *Appl. Surf. Sci.* **228**, 221–226 (2004).
26. Güdde, J., Hohlfeld, J., Müller, J. G. & Matthias, E. Damage threshold dependence on electron-phonon coupling in Au and Ni films. *Appl. Surf. Sci.* **127–129**, 40–45 (1998).

**Acknowledgements** This work was supported by the Creative Research Initiatives Program of the Ministry of Science and Technology in the Republic of Korea.

**Author Information** Reprints and permissions information is available at [www.nature.com/reprints](http://www.nature.com/reprints). Correspondence and requests for materials should be addressed to S.-W.K. (swk@kaist.ac.kr).